Journal of Alloys and Compounds 804 (2019) 331–338

Contents lists available at ScienceDirect

Journal of Alloys and Compounds

journal homepage: http://www.elsevier.com/locate/jalcom

Synthesis, extended and local crystal structure, and thermoelectric properties of $Fe_{1-x}Re_xGa_3$ solid solution

Maxim S. Likhanov [a], Vladislav O. Zhupanov [a], Valeriy Yu Verchenko [a, b], Andrei A. Gippius [c, d], Sergei V. Zhurenko [c, d], Alexey V. Tkachev [c], Dina I. Fazlizhanova [d], David Berthebaud [e, f], Andrei V. Shevelkov [a, *]

[a] Department of Chemistry, Lomonosov Moscow State University, Moscow, 119991, Russia
[b] National Institute for Chemical Physics and Biophysics, Tallinn, 12618, Estonia
[c] Faculty of Physics, Lomonosov Moscow State University, Moscow, 119991, Russia
[d] P.N. Lebedev Physics Institute RAS, Moscow, 119991, Russia
[e] Laboratoire CRISMAT, UMR 6508 CNRS/ENSICAEN, F-14050, Caen Cedex 4, France
[f] CNRS-Saint Gobain-NIMS, UMI 3629, Laboratory for Innovative Key Materials and Structures (LINK), National Institute for Materials Science, Tsukuba, 305-0044, Japan

ARTICLE INFO

Article history:
Received 11 April 2019
Received in revised form
2 July 2019
Accepted 3 July 2019
Available online 4 July 2019

Keywords:
Intermetallics
Rhenium
Thermoelectric
NQR spectroscopy
Solid solution

ABSTRACT

We present a new $Fe_{1-x}Re_xGa_3$ solid solution, in which a 5*d*-metal−−rhenium−−partially substitutes for iron to the limiting composition of $x = 0.10$. The crystal structure refined for the composition $Fe_{0.91}Re_{0.09}Ga_3$ shows the expected increase in the unit cell parameters compared to the parent $FeGa_3$ compound, however the M−M (M = Fe, Re) distance decreases within the M−M dumbbell, indicating an increased M−M bonding density. Therein, investigation of the local structure by means of ^{69,71}Ga NQR spectroscopy revealed the formation of homonuclear Fe−Fe and Re−Re dumbbells. Transport and thermoelectric properties have been investigated for the Re-substituted $FeGa_3$. Electrical transport measurements showed preservation of the nonmetallic conductivity of $Fe_{1-x}Re_xGa_3$ despite the decrease of the valence electron concentration from 17 to 16.9 electrons per formula. At low temperatures, $Fe_{1-x}Re_xGa_3$ is a *p*-type semiconductor with the band gap of 0.4 eV, but with increasing temperature the sign of the dominant charge carriers changes. Owing to the alloying effect, $Fe_{1-x}Re_xGa_3$ displays 1.5 times lower thermal conductivity than $FeGa_3$, which increases at high temperatures because of the growing contribution of the electronic term.

1. Introduction

Compounds of the $IrIn_3$ structure type family belong to the class of intermetallics formed by *d*-block metals and metals or semimetals of the *p*-block of the Periodic Table. Peculiarities of the electronic structure of these compounds are caused by an overlap of the transition atom *d*-orbitals with *s*-, *p*-orbitals of the p-element and lead to the energy gap opening in the band structure [1]. If the Fermi level falls into the gap, a compound demonstrates semiconductor-like behavior. Evidently, the valence electron concentration (VEC) per one atom of the transition metal directly determines the type of conductivity of a compound. Compounds of this structure type with 17 valence electrons demonstrate semiconducting properties ($FeGa_3$, $RuGa_3$, $OsGa_3$, and $RuIn_3$) [1–4], whereas those having 18 valence electrons are typical metals ($CoGa_3$, $RhGa_3$, $IrGa_3$, $CoIn_3$, $RhIn_3$, and $IrIn_3$) [1,5–8]. Interest in this family has increased in recent years due to intriguing thermoelectric properties: Compounds with 17 valence electrons, particularly $FeGa_3$, $RuGa_3$, and $RuIn_3$, have high Seebeck coefficient (of a few hundred $\mu V \cdot K^{-1}$) [3]. The features of the band structure such as narrow peaks of the density of states in the vicinity of the Fermi energy are favorable for high thermoelectric performance, which can be tuned and adjusted by performing various-type doping [9,10]. Moreover, a chemical modification, namely the creation of solid solutions, allows the reduction of absolute values of electrical resistivity and thermal conductivity, which are unsuitably high for the unsubstituted 17e-compounds. Particularly, partial substitution of zinc for indium in $RuIn_3$ results in high thermoelectric figure-of-

* Corresponding author.
E-mail address: shev@inorg.chem.msu.ru (A.V. Shevelkov).

https://doi.org/10.1016/j.jallcom.2019.07.033
0925-8388/

merit, $ZT = 0.8$ at 620 K [11].

$FeGa_3$ holds a special place among all representatives of the $IrIn_3$ structure type. On the one hand, $FeGa_3$ possesses promising thermoelectric parameters such as the abnormally high Seebeck coefficient [12], which is a consequence of the phonon-drag effect and which can be used to create thermoelectric materials; on the other hand, $FeGa_3$-based solid solutions are of great fundamental interest in terms of the influence of various substitutions on functional properties. For instance, *n*-doping in $FeGa_3$ affects properties differently depending on which position the substitution occurs in. Specifically, substitution in the Fe sublattice leads to a smooth transition to the metallic state, which was demonstrated for the $Fe_{1-x}M_xGa_3$ (M = Co, Ni) solid solutions [13–15], where the transition occurs at the concentration of a dopant ranging from 2.5 to 5%. Along with that, although weak antiferromagnetic correlations in the case of Ni-substituted sample were observed, no magnetic ordering appears [15]. Quite the reverse, substitution in the Ga sublattice by germanium causes an instantaneous transition to the metallic state at the lowest degree of substitution; moreover, at the concentration of germanium $y > 0.13$ the $FeGa_{3-y}Ge_y$ solid solution develops quantum critical behavior accompanied by a transition into the ferromagnetically ordered state [16–20]. In addition, substitutions with an increase in the number of valence electrons basically coincides with the prediction within the rigid-band model, according to which the Fermi level shifts from the band gap toward the conduction band, whereas *p*-doping in $FeGa_3$ proceeds without any change in semiconducting properties, up to the maximum degrees of substitution in both iron and gallium sublattices, which was shown for the $Fe_{1-x}Mn_xGa_3$ and $FeGa_{3-y}Zn_y$ solid solutions [21]. A true nature of this behavior remains unclear; however, the reason seems to lie in the peculiarities of the real crystal and electronic structure of $FeGa_3$. Thus, the in-gap states were detected in the band structure of $FeGa_3$ [22], which are possibly associated with Fe–Fe dangling bonds or the presence of the additional iron atoms [23].

Recent studies show that the substitution in $FeGa_3$ causes a regular semiconductor-to-metal transition in the case of *n*-doping, as was shown for $Fe_{1-x}M_xGa_3$ (M = Co, Ni) and $FeGa_{3-y}E_y$ (E = Ge, Sn) solid solutions [13–20,24,25]. The only two known *p*-type solid solutions ($Fe_{1-x}Mn_xGa_3$ and $FeGa_{3-y}Zn_y$) behave differently: the in-gap states are introduced as a result of doping, which remain localized even at the maximum degree of substitution [21,25]. Thus, no semiconductor-to-metal transition occurs in the case of *p*-doping. It is curious to note that substitution in $FeGa_3$ without changing the VEC occurs with preservation of semiconducting behavior in the case of the $FeGa_{3-y}Al_y$ solid solution [26], in which the replacement of gallium by aluminum atoms is a chemical analogue of pressure, which should lead to the energy gap closure and metallic conductivity [27]. The main factors that govern the physical properties of $FeGa_3$ and other $IrIn_3$-type intermetallics remain largely unexplored. In this light, the isoelectronic substitutions by atoms with the same electronic configuration of the outer shell but with different sizes may help in establishing the general trends of how the real crystal and electronic structure are connected with physical properties through the valence electron concentration. In particular, functional properties may be rationalized and optimized for $FeGa_3$ and $IrIn_3$-type intermetallics in general.

In this work, we present an investigation of a new *p*-type solid solution $Fe_{1-x}Re_xGa_3$. We report its homogeneity region, results of the study of the local and extended crystal structure by X-ray diffraction (XRD) using synchrotron radiation and by nuclear quadrupole resonance (NQR) spectroscopy, as well as thermoelectric properties in the mid-temperature region and compare our results with the related $Fe_{1-x}Mn_xGa_3$ system.

2. Experimental section

2.1. Synthesis

Synthesis of the samples with the composition $Fe_{1-x}Re_xGa_3$ where $x = 0.01, 0.02, 0.03, 0.04, 0.05, 0.06, 0.07, 0.08, 0.09, 0.10, 0.11$, and 0.15 was carried out utilizing a two-step ampoule technique using Fe (Acros Organics, 99.9%) and Re (Alfa Aesar, 99.99%) powders and Ga grains (Sigma Aldrich, 99.999%) as starting materials. The first stage included annealing of the stoichiometric amounts of the initial metals in quartz ampoules sealed under vacuum at 750 °C for a week. On the second stage, the obtained samples were crushed using an agate mortar and a pestle, compressed into pellets at room temperature and subjected to another annealing under the same conditions. The powders obtained by grinding the pellets were used for the investigation by XRD and NQR spectroscopy methods and for the study of the thermoelectric properties.

2.2. Phase and elemental composition and crystal structure investigation

Phase composition of the products was determined by powder X-ray diffraction (PXRD) analysis using a Huber G670 Guinier Camera ($CuK\alpha_1$ radiation, Ge monochromator, $\lambda = 1.5406$ Å). Elemental germanium was used as an internal standard in the profile analysis and unit cell parameters calculations. Determination of the chemical composition of the pressed pellets of the $Fe_{1-x}Re_xGa_3$ solid solution samples was carried out using a scanning electron microscope JSM JEOL 6490-LV equipped with an energy dispersive X-ray (EDX) analysis system INCA x-Sight. EDX analysis demonstrated that for all samples within the homogeneity range the observed Fe:Re ratio exactly matched the nominal composition. For the sample with the higher rhenium content, the presence of the impurity phase, $ReGa_5$ [28], was detected (Fig. 1). Crystal structure refinement (Tables 1 and 2) was performed using high-resolution PXRD data assembled at the ID22 beamline of the European Synchrotron Radiation Facility (ESRF) ($\lambda = 0.35422$ Å, $2\theta_{max} = 34$ deg.). Room and high temperature measurements were performed on powder samples enclosed in sealed quartz capillaries with an inner diameter of 0.4 mm. The capillaries were spun during the measurement. A programmable blower was used to heat the samples. Jana 2006 software was used for the structure refinement [29].

2.3. Nuclear quadrupole resonance spectroscopy

The ^{69,71}Ga nuclear quadrupole resonance (NQR) measurements were performed at 77 K utilizing a home-built phase coherent pulsed NQR spectrometer with direct digital quadrature detection at the carrier frequency. The ^{69,71}Ga NQR spectra were measured using a frequency step point-by-point spin-echo technique. At each frequency point, the area under the spin-echo magnitude was integrated in the time domain and averaged by a number of accumulations, which depends on the Ga isotope and frequency. Alternatively, we used a Fourier transform summation (FTS) method for spectra accumulation since the ^{69,71}Ga NQR lines are rather broad [30].

2.4. Thermoelectric properties measurements

For thermoelectric properties measurements, pellets of the $Fe_{1-x}Re_xGa_3$ solid solution with $x = 0.04$ and 0.08 were prepared by SPS technology using a Labox-625 (Sinter Land) machine. Densification was carried out in cylindrical graphite dies with the inner diameter of 10 mm by heating the sample to 973K under a pressure of 60 MPa

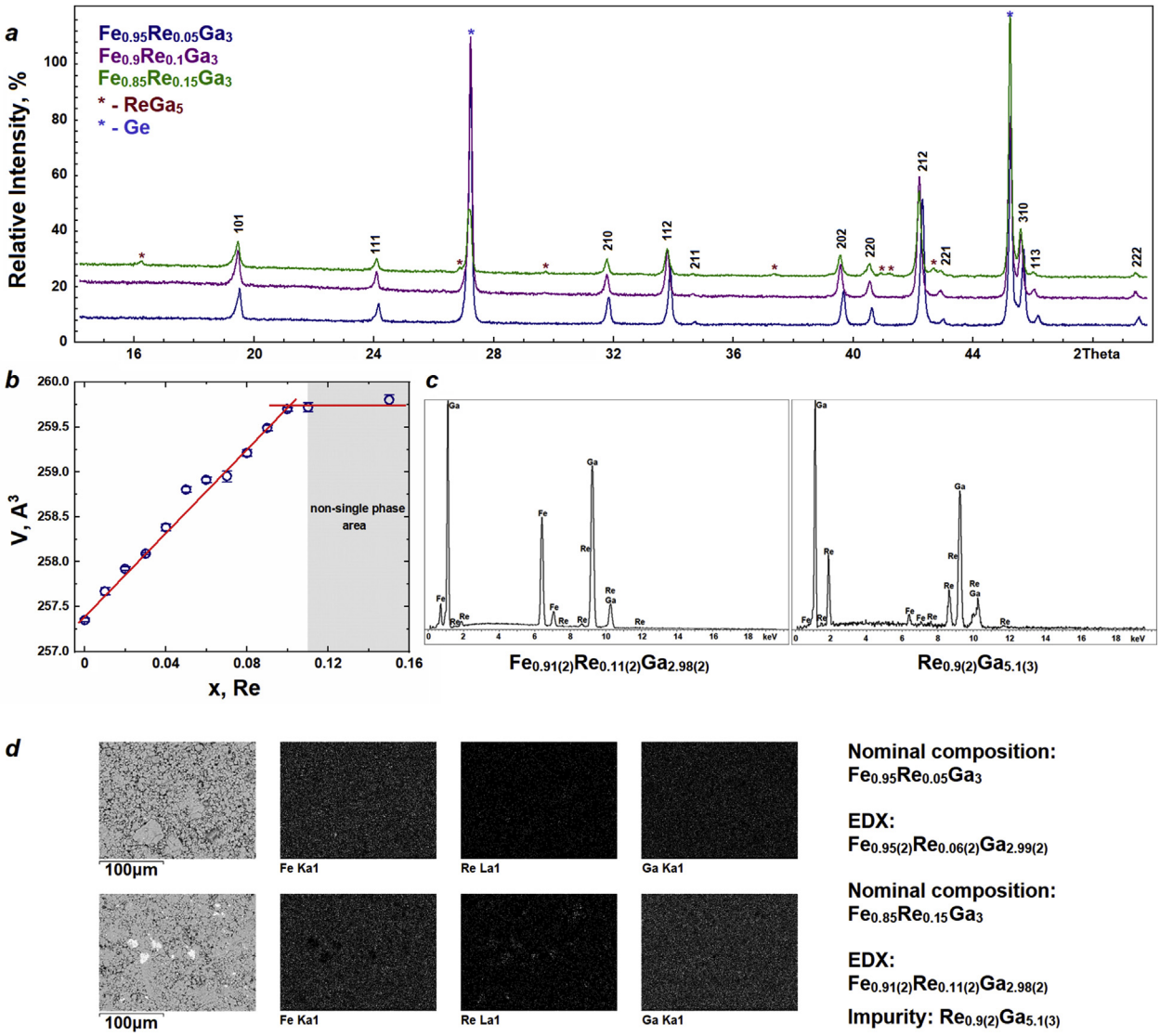

Fig. 1. ***a*** – PXRD patterns of the $Fe_{1-x}Re_xGa_3$ samples ($x = 0.05$, 0.1, and 0.15). ***b*** – dependence of the unit cell volume of the $Fe_{1-x}Re_xGa_3$ solid solution on the nominal composition.***c*** – EDX spectrum for $Fe_{1-x}Re_xGa_3$ and impurity phase at $x = 0.15$.***d*** – EDX mapping of the $Fe_{1-x}Re_xGa_3$ samples with $x_{nom} = 0.05$ and 0.15.

Table 1
Crystallographic and refinement parameters for $Fe_{1-x}Re_xGa_3$, $x = 0.088(1)$.

Nominal composition	$Fe_{0.91}Re_{0.09}Ga_3$
Composition from refinement	$Fe_{0.912(1)}Re_{0.088(1)}Ga_3$
Crystal system	Tetragonal
Space group	$P4_2/mnm$
a, Å	6.27894(2)
c, Å	6.58395(2)
V, Å^3	259.573(1)
Z	4
d_{calc}, g/cm^3	7.073
Wavelength, Å	0.35422
Temperature, K	293
2θ range (data collection), °	1.00–35.00
R/*Rw*	0.0342/0.0400
GoF	1.83

in vacuum, keeping it at this temperature for 10 min, and then cooling down to room temperature. The relative density of the samples of approximately 98% was achieved. Pellets were cut into parallelepipeds with the sizes $0.8 \times 0.3 \times 0.2$ cm^3 and $0.6 \times 0.6 \times 0.1$ cm^3 for charge transport and thermal conductivity measurements, respectively.

Mid-temperature electrical resistivity and Seebeck coefficient were simultaneously measured with an ULVAC ZEM-3 system by using the four-probe method and differential method, respectively, at the 300–1000 K temperature range under partial pressure of helium. The thermal diffusivity was measured by the laser flash technique using a LFA-457 apparatus. The thermal conductivity was calculated from measured thermal diffusivity, specific heat capacity, and sample density. Specific heat capacity was calculated according to Dulong-Petit law.

3. Results and discussion

3.1. Synthesis, homogeneity range, and crystal structure

Substitution of Re for Fe leads to the formation of the $Fe_{1-x}Re_xGa_3$ solid solution, where x_{max} lies near 0.1: PXRD analysis of the samples demonstrates the presence of a single phase at $x \leq 0.1$, with the unit cell parameters and volume increasing linearly with the

Table 2
Atomic parameters for $Fe_{1-x}Re_xGa_3$, $x = 0.088(1)$.

Atom	Wyckoff site	x	y	z	Occupancy	U_{iso}, Å^2
M1	4*f*	0.34481(7)	0.34481(7)	0	0.912(1)Fe + 0.088(1)Re	0.0028(3)
Ga1	4*c*	0	0.5	0	1	0.0078(2)
Ga2	8*j*	0.15593(6)	0.15593(6)	0.26180(9)	1	0.0071(2)

nominal rhenium content. For the samples with $x > 0.1$ the unit volume does not change and the presence of the $ReGa_5$ impurity phase is observed (Fig. 1). The results of the phase analysis are in good agreement with the data of elemental analysis by EDXs. The observed composition of $Fe_{1-x}Re_xGa_3$ coincides with the nominal ratio of elements within the measurement error. The mapping of elements across the surface demonstrates homogeneous distribution of Fe, Re, and Ga. The $ReGa_5$ phase was detected as an impurity phase at $x > 0.1$. The observed homogeneity region is very close to that found for the solid solution formed by partial substitution of manganese for iron in $FeGa_3$ ($x_{max} < 0.12$ [21]). Given that the covalent radii of iron and manganese are very close to each other and that of rhenium is significantly higher, ($r_{cov}(Fe) = 1.165$ Å, $r_{cov}(Mn) = 1.17$ Å, $r_{cov}(Re) = 1.28$ Å), the size factor is not the predominate one in setting the compositional limit of the solid solution. Both Mn and Re lead to the change of the VEC from 17 in binary $FeGa_3$ to about 16.9 electrons per formula in the solid solutions, hinting that the electronic factor seems to be more significant. This is true not only for *p*-doping. It is known from the literature that iron in $FeGa_3$ can be completely replaced by cobalt, whereas substitution by nickel is limited to 4% [15]. The latter is probably associated with the difference in the electronic structure of cobalt and nickel since their covalent radii are too similar and cannot explain their different solubility in $FeGa_3$. Specifically, the difference can be associated with the effective $3d^{10}$ electronic configuration of nickel forming bonds with less electronegative gallium.

The crystal structure was refined for the sample with the nominal composition of $Fe_{0.91}Re_{0.09}Ga_3$, lying very close to the solubility limit. The refinement was performed against the high-resolution data collected using synchrotron radiation (Fig. 2). Phase analysis showed the $FeGa_3$-based phase along with unreacted Re metal, which amount is ~0.3 mass. % according to the Rietveld refinement. It should be noted that the Re admixture is not visible in the laboratory XRD and EDX measurements, and its small amount do not contribute to the determined homogeneity range within the standard deviation of the EDXs measurements. Further analysis of the PXRD pattern presented in Fig. 2 showed that the solid solution retains the crystal structure of the parent binary compound. No superstructure reflections indicating possible ordering of rhenium and iron atoms were observed. Therefore, the initial atomic parameters were taken from the crystal structure of $FeGa_3$, and the solution converged giving the refined composition $Fe_{0.912(1)}Re_{0.088(1)}Ga_3$ matching the initial composition within the accuracy of determination. PXRD patterns taken in the range of 300–800 K showed no change in the crystal structure as indicated by the linear dependence of the unit cell volume upon temperature (Fig. 3). Further details on the crystal structure investigation may be obtained from the Cambridge Crystallographic Data Centre by quoting the CCDC accession code 1903276.

The crystal structure of $FeGa_3$ (Fig. 4) contains pairs of iron atoms forming Fe–Fe dumbbells in the prismatic surrounding of Ga2 atoms. Compared to the crystal structure of parent $FeGa_3$, the interatomic distance in such dumbbells for the $Fe_{0.912(1)}Re_{0.088(1)}Ga_3$ turns out to be a bit smaller, 2.756(1) Å vs. 2.776(1) Å (see Table 3), despite the general increase in the unit cell parameters and volume. This distance is even shorter than those found in the $Fe_{1-x}Co_xGa_3$ and $Fe_{1-x}Ni_xGa_3$ solid solutions, in which smaller cobalt or nickel substitute for iron [31]. This result may indicate an increase in the bonding density between the transition metal atoms in the dumbbells in the substituted compound compared to $FeGa_3$. However, substitution of Re for Fe in the crystal structure of $FeGa_3$ may proceed in two different modes, because from the crystallographic point of view this substitution may result locally in formation of Fe–Re or Re–Re dumbbells along with preservation of the majority of Fe–Fe dumbbells. In our previous study we showed that Fe–Fe and Co–Co dumbbells are strongly preferred to the Fe–Co ones although the latter also exist in a quantity sufficient to be detected by ^{69,71}Ga NQR spectroscopy [32]. The local surrounding of the gallium atoms in the $FeGa_3$ structure can be characterized as follows (Fig. 4, panels *b* and *c*): Ga1 atom is located in a slightly distorted cube of eight Ga2 atoms, and its coordination is

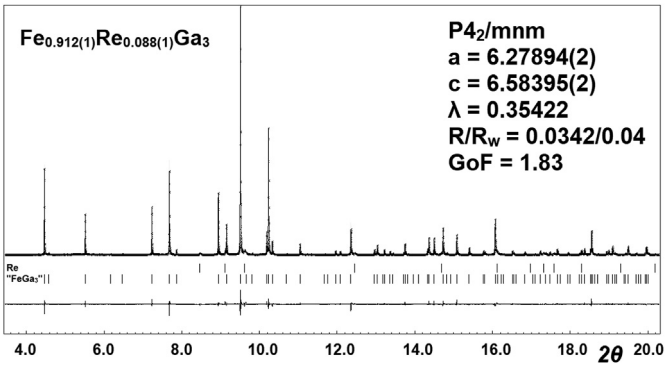

Fig. 2. Synchrotron PXRD pattern of the sample with the nominal composition $Fe_{0.91}Re_{0.09}Ga_3$. The upper line is the experimental pattern, the black ticks show peak positions of $Fe_{0.91}Re_{0.09}Ga_3$ and rhenium impurity, and the lower line is the difference between the calculated and experimental patterns.

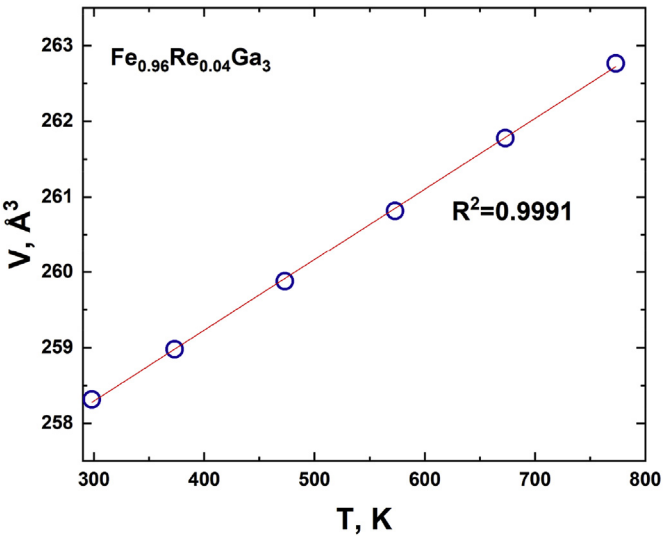

Fig. 3. Temperature dependence of the unit cell volume of the $Fe_{0.96}Re_{0.04}Ga_3$ sample.

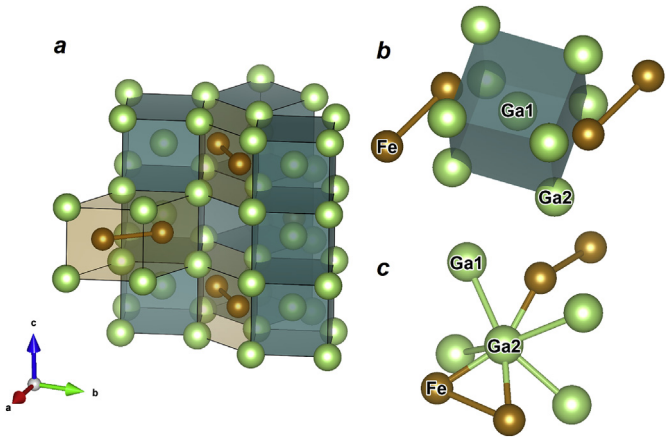

Fig. 4. ***a*** – polyhedral representation of the $FeGa_3$ crystal structure by columns of cubs $Ga1@Ga2_8$ and adjoined prisms $Fe_2@Ga2_8$. Environment of the Ga1 (***b***) and Ga2 (***c***) atoms.

Table 3
Selected interatomic distances for $Fe_{0.912(1)}Re_{0.088(1)}Ga_3$. M = 0.912(1)Fe + 0.088(1) Re.

Atom	Atom	Distance, Å
M –	Ga1 (× 2)	2.3742(5)
	Ga2 (× 2)	2.4050(6)
	Ga2 (× 4)	2.5051(6)
	M (× 1)	2.7560(6)
Ga1 –	Ga2 (× 4)	2.8435(5)
	Ga2 (× 4)	2.9321(5)
Ga2 –	Ga2 (× 1)	2.7693(6)

supplemented by Fe atoms joined into the Fe–Fe dumbbells and directed opposite and parallel each other relative to the Ga1 atom. Ga2 atom is located in a less symmetric surrounding and is bound with the dumbbell of iron atoms in a side mode and one more iron atom, which is included in another dumbbell located perpendicular to the first one. Substitution of Re for Fe evokes changes in a local structure of gallium atoms, which can be probed by NQR spectroscopy.

3.2. Local crystal structure by NQR spectroscopy

The experimental ^{69}Ga NQR spectra for the solid solution samples with the composition $Fe_{0.92}Re_{0.08}Ga_3$ and $Fe_{0.96}Re_{0.04}Ga_3$ are shown in Fig. 5. Two intense narrow peaks with the resonance frequencies of 35.0 and 41.9 MHz and two less intense peaks with the frequencies of 41.1 and 47.6 MHz are found in the spectra. The difference between the frequencies observed for the two samples is minimal; the shift of the spectral line is only 20–60 kHz. The observed picture contrasts with that found for $FeGa_3$ and $Fe_{1-x}M_xGa_3$ (M = Co and Ni) [15]. For the binary compound, the ^{69}Ga NQR spectrum consists of two very narrow sharp peaks reflecting two positions of gallium atoms. For the $Fe_{1-x}M_xGa_3$ (M = Co and Ni) solid solutions, line broadening and a complex pattern of wide peaks appear, reflecting multifold local surrounding of gallium. Surprisingly, partial substitution of iron by rhenium leads to an intermediate type of the NQR spectrum, showing more uniform surrounding of gallium atoms by transition metal dumbbells. Given that only 4–8% of iron is replaced by rhenium, two rather narrow intense peaks can be attributed to Ga(1) and Ga(2) atoms bound to undisturbed Fe–Fe dumbbells, where the greater degree of substitution results in wider peaks due to the greater disorder introduced by local nonequivalence of Ga atoms

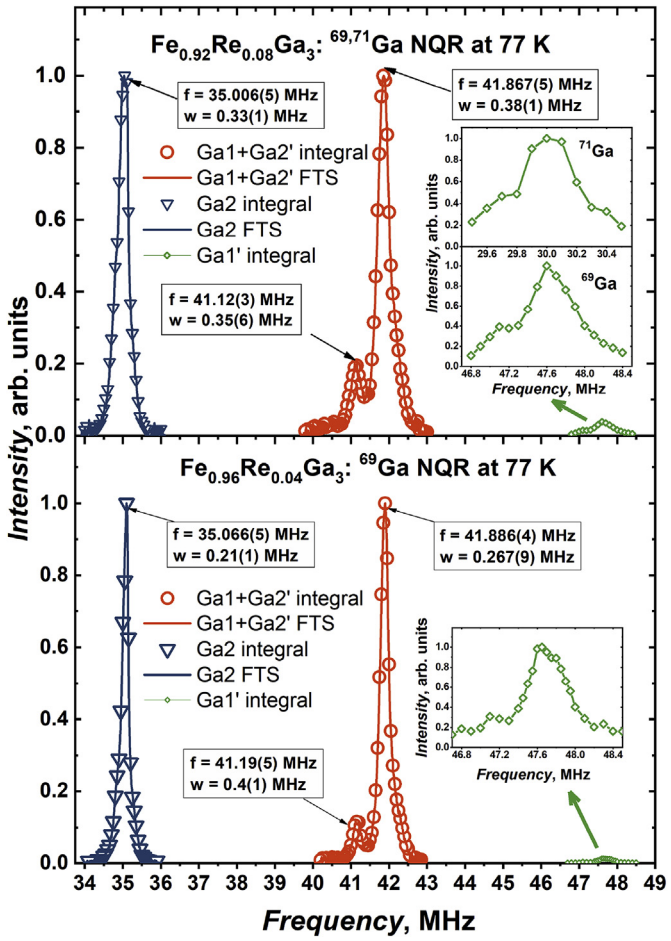

Fig. 5. Normalized ^{69}Ga NQR spectra at the Ga1 and Ga2 sites for $Fe_{0.92}Re_{0.08}Ga_3$ (top) and $Fe_{0.96}Re_{0.04}Ga_3$ (bottom) measured at 77K. Symbols correspond to spin-echo integration method; green solid line – Fourier transform summation (FTS) method. Inserts show $^{69,71}Ga$ (Re 8%) and ^{69}Ga (Re 4%) NQR satellites of the lowest intensity. (For interpretation of the references to colour in this figure legend, the reader is referred to the Web version of this article.)

coordination. Then, the smaller and wider additional peaks at 41.1 and 47.6 MHz can be attributed to gallium atoms that contact with rhenium atoms of the Re–Re or Fe–Re dumbbells. To confirm that the small high-frequency NQR line at 47.6 MHz indeed originates from the ^{69}Ga nuclei we measured the corresponding line from the ^{71}Ga isotope at 30 MHz (Fig. 5, Insert in the upper panel) and found that the frequency ratio perfectly matches the ratio of the quadrupole moments $Q(^{69}Ga)/Q(^{71}Ga) = 1.60$. Apparently, on going from 8% to 4% of Re for Fe substitution the intensity of smaller peaks decreases reflecting the smaller number of gallium atoms contacting with rhenium atoms. To shed light on the nature of such dumbbells, we performed calculation of resonant frequencies for binary $FeGa_3$ and $ReGa_3$ using the crystal structures of $FeGa_3$ and $ReGa_3$ reported in the literature as the starting model for geometry optimization [32,33]. Comparison of the observed (Fig. 5) and

Table 4
Calculated ^{69}Ga NQR frequencies for $FeGa_3$ and $ReGa_3$ compounds.

Compound	Ga site	ν_Q calculated, MHz
$FeGa_3$	Ga1	39.91 [32]
	Ga2	33.91 [32]
$ReGa_3$	Ga1	49.1
	Ga2	45.9

calculated (Table 4) frequencies hints for the presence of homonuclear Re–Re dumbbells because the additional signals are expectedly observed at higher frequencies and they are relatively narrow showing no distribution expected in the case of Fe–Re dumbbells. We note that the Re–Re distance of 2.756 Å, which should be assumed in the case of Re–Re dumbbells, is not too short; it nicely corresponds to the interatomic distances in the crystal structure of Re metal, 2.745–2.766 Å [34], whereas optimization of the imaginary crystal structure of WGa_3 predicts even shorter contacts of 2.532 Å between adjacent atoms of tungsten – a neighbor of rhenium in the 6th period of the Periodic table [35].

3.3. Thermoelectric properties

The temperature dependences of the electrical resistivity, Seebeck coefficient, thermal conductivity, and thermoelectric figure-of-merit for $Fe_{1-x}Re_xGa_3$ with $x = 0.04$ and 0.08 in the temperature range from 300 to 1000 K are presented in Fig. 6. For both samples, a semiconducting conductivity character and an exponential resistivity drop with the increasing temperature are observed, with the calculated band gap width being about 0.4 eV. The composition with higher rhenium content, $x = 0.08$, is characterized by lower absolute values of resistivity, indicating an increase in the charge carrier concentration in comparison with the sample containing less rhenium, $x = 0.04$. Similar behavior is observed for the absolute values of the Seebeck coefficient. At temperatures of 300–400 K the sample with $x = 0.04$ possesses high thermopower of about 200 μV/K, which is 3–4 times greater than for the composition with $x = 0.08$. Both samples display positive Seebeck coefficient, showing that holes are the dominant charge carriers. However, as the temperature increases the Seebeck coefficient decreases, changes its sign near 550 K ($x = 0.08$) or 620 K ($x = 0.04$), and then attains the constant value of nearly −30 μV/K for both samples. The sign change of the Seebeck coefficient indicates that the type of dominant charge carriers changes from holes to electrons at high temperatures. Similar behavior was observed in the isomorphous Ru-based compounds, – in $RuGa_3$ [3,4,36,37], where the Seebeck coefficient changes its sign from negative to positive at $T \sim 500$ K, and in $RuIn_3$, for which Hall measurements indicate that holes rather than electrons act as major charge carriers at temperatures above $T \sim 325$ K [31,38]. The change between the *p*-type and *n*-type transport occurring at the elevated temperatures in $RuGa_3$ and $RuIn_3$ is associated with the multiple-band behavior of these compounds. For instance, in the electronic structure of $RuIn_3$, the bottom of the conduction band is presented by two minima with substantially different effective electron masses. The small energy difference between these minima yields the two-band transport at the elevated temperatures accompanied by the change from the *n*-type to *p*-type conductivity [38]. In $RuGa_3$, which also has such electronic structure features, semiclassical Boltzmann theory-based calculations of transport properties reproduce well the experimental $S(T)$ behavior including the change of sign [4]. For $Fe_{1-x}Re_xGa_3$, we assume that the observed sign change is also associated with the multiple-band transport that originates from the peculiarities of the electronic structure. This way, the temperature, at which the sign change occurs, 550 K for $x = 0.08$ and 620 K for $x = 0.04$, should depend on the energy difference between two electronic bands having different effective masses. However, it is difficult to establish fine details of the electronic structure of $Fe_{1-x}Re_xGa_3$ taking into account that the system clearly does not follow the rigid band behavior.

It is still not clear whether the conservation of the semiconducting properties is a specific feature of *p*-doping in $FeGa_3$ or a consequence of the real $FeGa_3$ electronic structure. A simple approach of rigid zones results in the transition to the metallic state

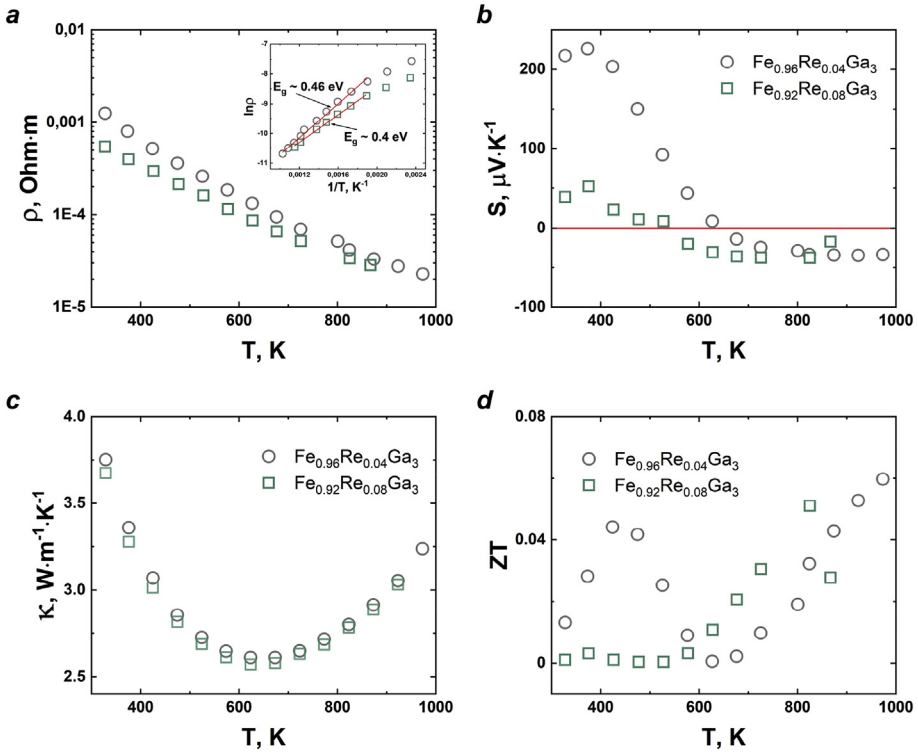

Fig. 6. Temperature dependences of electrical resistivity (***a***), Seebeck coefficient (***b***), thermal conductivity (***c***), and thermoelectric figure-of-merit (***d***) for $Fe_{1-x}Re_xGa_3$ ($x = 0.04$ and 0.08).

after the Re for Fe substitution, which is not confirmed in our experiments.

Transport properties of $Fe_{1-x}Re_xGa_3$ can be compared with those of $Fe_{1-x}Mn_xGa_3$ published by Gamza et al. [21]. They found that even at the maximum doping level of $x = 0.12$ no semiconductor-to-metal transition takes place, and above 60 K the activated temperature dependence of resistivity is observed, which they attributed to the localized nature of acceptor-type states. The latter was confirmed by band structure calculations accounting for electron correlations, which revealed localization of holes on Mn centers and opening of a band gap even at an imaginary substitution level of $x = 0.25$. Taking into account donor-type impurities assembled as in-gap states in pristine $FeGa_3$, which could be associated with dangling Fe–Fe bonds, multiple band behavior of $Fe_{1-x}Mn_xGa_3$ and $Fe_{1-x}Re_xGa_3$ should be expected, leading to a change in the sign of the Seebeck coefficient. Unfortunately, the temperature dependence of the Seebeck coefficient was not reported for $Fe_{1-x}Mn_xGa_3$; therefore, it cannot be compared with our data on $Fe_{1-x}Re_xGa_3$. However, we note that a similar change of the sign on the *S(T)* curve was previously reported for $Ru_{1-x}In_3$ (including $x = 0$) and $RuGa_3$ having the same crystal structure [3,4,36].

Thermal conductivity of both samples lies in the range of 2.5–3.75 $Wm^{-1}K^{-1}$, and the difference between the two samples is only marginal. The thermal conductivity decreases from 3.75 $Wm^{-1}K^{-1}$ at room temperature to the minimum observed at 620 K (~2.5 $Wm^{-1}K^{-1}$) and then increases reaching 3.2 $Wm^{-1}K^{-1}$ at 973 K (Fig. 6). Such a parabolic-like behavior of $\kappa(T)$ with a pronounced minimum was previously reported for *n*-type $Fe_{1-x}M_xGa_3$ (M = Co, No), where the minimum on the $\kappa(T)$ function almost coincides with the temperature of the metal-to-semiconductor transition [15]. In the present study, we did not observe this kind of transition, nor did we detect any structural changes in the investigated temperature range (see Fig. 3). We infer that the upturn at high temperatures stems from the increasing electronic contribution (κ_e) to the total thermal conductivity. In this work, κ_e was calculated according to Wiedemann-Franz law as $\kappa_e = L_0 T \rho^{-1}$, assuming the temperature independent ideal Lorentz number $L_0 = 2.45\ 10^{-8}\ V^2K^{-2}$, and was found to grow substantially with temperature. At 300 K it constitutes not more than 2% of the total thermal conductivity but as the temperature tends to 1000 K this contribution becomes pronounced, reaching 30% of the total thermal conductivity (Fig. 7). Since the lattice (phonon) contribution expectedly decreases with temperature, the increasing electronic part ensures increasing of the total thermal conductivity after 620 K for both samples.

Absolute values of the thermal conductivity of $Fe_{1-x}Re_xGa_3$ ($x = 0.04$ and 0.08) are less than those for pure $FeGa_3$ (2.8–4.1 $Wm^{-1}K^{-1}$ in the same temperature region [24,25]). In Fig. 7, the total thermal conductivity is divided into two parts highlighting the lattice and electronic contributions. By comparing our data with literature, it becomes obvious that the reduction of thermal conductivity of $Fe_{1-x}Re_xGa_3$ is provided mainly by the suppression of the lattice part, while the calculated electronic contribution is somewhat higher than that of unsubstituted $FeGa_3$, which is associated with the increase of electrical conductivity of $Fe_{1-x}Re_xGa_3$. The reduced lattice thermal conductivity occurs due to the effect of doping by heavy rhenium atoms and by the alteration of Fe–Fe and Re–Re dumbbells in the crystal structure, which intensifies phonon scattering, but in general the measured values of κ are typical for materials based on $FeGa_3$ [14,24,25,39].

As a result of the non-monotonic changes of the Seebeck coefficient and thermal conductivity the thermoelectric figure-of-merit *ZT* possesses complex temperature dependence (Fig. 6). *ZT* increases with temperature passing local extrema corresponding to the temperatures of the Seebeck coefficient sign change and of the thermal conductivity change. The maximum value is $ZT = 0.06$ at 975 K for the $Fe_{0.96}Re_{0.04}Ga_3$ composition.

4. Conclusions

In summary, $Fe_{1-x}Re_xGa_3$ is a new solid solution that forms upon substituting Re for Fe in the semiconducting intermetallic compound $FeGa_3$. The substitution limit of $x = 0.1$ is very close to that previously found for $Fe_{1-x}Mn_xGa_3$; taking into account the size difference of Mn and Re, we infer that the electronic factor prevails over the size factor in determining the limit of the homogeneity range. The local structure investigation reveals the formation of Re–Re homoatomic dumbbells manifested as a set of well-shaped additional peaks in the ^{69}Ga NQR spectra corresponding to two gallium positions adjacent to Re atoms. $Fe_{1-x}Re_xGa_3$ solid solution retains non-metallic properties thus violating predictions made using the rigid band approach. At low temperatures, the solid solution has a band gap of about 0.4 eV in its electronic structure and exhibits the *p*-type conductivity. As the temperature increases, the sign of the dominant charge carriers changes from holes to electrons. The thermal conductivity of $Fe_{1-x}Re_xGa_3$ is 2–3 times less that in parent $FeGa_3$ owing to the alloying effect, e.g. alteration of the Fe–Fe and Re–Re dumbbells that enhances scattering of phonons. The resulting maximum value of the thermoelectric figure-of-merit of $Fe_{1-x}Re_xGa_3$ remains relatively low, $ZT = 0.06$ at 975 K for $x = 0.04$. Our results indicate that $FeGa_3$ is a peculiar intermetallic compound showing that the details of the local crystal and electronic structure make great impact on the properties. They include alternation of the dumbbells, in-gap states, on-site defects, and others that are not yet understood; however, their clarification is

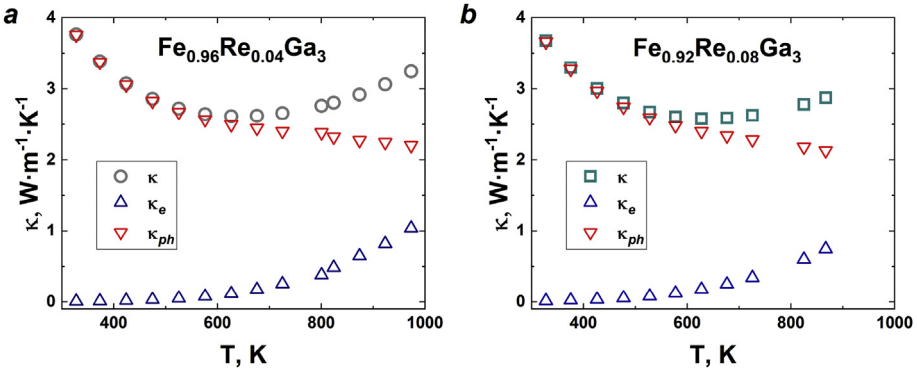

Fig. 7. Thermal dependencies of total (κ) thermal conductivity and electronic (κ_e) and lattice (κ_{ph}) contributions for $Fe_{0.96}Re_{0.04}Ga_3$ (***a***) and $Fe_{0.92}Re_{0.08}Ga_3$ (***b***).

crucial for achieving high thermoelectric performance of $FeGa_3$-based materials.

Acknowledgments

We acknowledge ESRF for granting the beam time at ID22 and thank W. Mogodi for his kind support during the high-resolution XRD measurement. We acknowledge the use of the SPS machine purchased under the Program of Development of Lomonosov Moscow State University. This work is supported by the Russian Foundation for Basic Research, grants Nos. 16-53-52012 and 17-03-00111.

Appendix A. Supplementary data

Supplementary data to this article can be found online at https://doi.org/10.1016/j.jallcom.2019.07.033.

References

[1] U. Häussermann, M. Boström, P. Viklund, Ö. Rapp, T. Björnängen, $FeGa_3$ and $RuGa_3$: semiconducting intermetallic compounds, J. Solid State Chem. 165 (2002) 94–99.
[2] Y. Imai, A. Watanabe, Electronic structures of semiconducting $FeGa_3$, $RuGa_3$, $OsGa_3$, and $RuIn_3$ with the $CoGa_3$- or the $FeGa_3$-type structure, Intermetallics 14 (2006) 722–728.
[3] Y. Amagai, A. Yamamoto, T. Iida, Y. Takanashi, Thermoelectric properties of semiconductorlike intermetallic compounds $TMGa_3$ (TM = Fe, Ru, and Os), J. Appl. Phys. 96 (2004) 5644–5648.
[4] Y. Takagiwa, K. Kitahara, Y. Matsubayashi, K. Kimura, Thermoelectric properties of $FeGa_3$-type narrow-bandgap intermetallic compounds $Ru(Ga,In)_3$: experimental and calculational studies, J. Appl. Phys. 111 (2012) 123707.
[5] N. Haldolaarachchige, W.A. Phelan, Y.M. Xiong, R. Jin, J.Y. Chan, S. Stadler, P. Young, Thermoelectric properties of intermetallic semiconducting $RuIn_3$ and metallic $IrIn_3$, J. Appl. Phys. 113 (2013) 08379.
[6] P. Viklund, S. Lidin, P. Berastegui, U. Häussermann, Variations of the $FeGa_3$structure type in the systems $CoIn_{3-x}Zn_x$ and $CoGa_{3-x}Zn_x$, J. Solid State Chem. 164 (2002) 100–110.
[7] R. Pöttgen, R.D. Hoffmann, G. Kotzyba, Structure, chemical bonding, and properties of $CoIn_3$, $RhIn_3$, and $IrIn_3$, Z. Anorg. Allg. Chem. 624 (1998) 244–250.
[8] J.C. Alvarez-Quiceno, G.M. Dalpian, A. Fazzio, J.M. Osorio-Guillen, Semiclassical transport properties of $IrGa_3$: a promising thermoelectric material, J. Phys. Condens. Matter 30 (2018) 085701.
[9] J.M. Osorio-Guillén, Y.D. Larrauri-Pizarro, G.M. Dalpian, Pressure-induced metal-insulator transition and absence of magnetic order in $FeGa_3$ from a first-principles study, Phys. Rev. B 86 (2012) 235202.
[10] A.S. Botana, Y. Quan, W.E. Pickett, Disturbing the dimers: electron and hole doping in the intermetallic insulator $FeGa_3$, Phys. Rev. B 92 (2015) 155134.
[11] D. Kasinathan, M. Wagner, K. Koepernik, R. Cardoso-Gil, Yu Grin, H. Rosner, Electronic and thermoelectric properties of $RuIn_{3-x}A_x$ (A = Sn, Zn), Phys. Rev. B 85 (2012) 035207.
[12] M. Wagner-Reetz, D. Kasinathan, W. Schnelle, R. Cardoso-Gil, H. Rosner, Yu Grin, P. Gille, Phonon-drag effect in $FeGa_3$, Phys. Rev. B 90 (2014) 195206.
[13] E.M. Bittar, C. Capan, G. Seyfarth, P.G. Pagliuso, Z. Fisk, Correlation effects in the small gap semiconductor $FeGa_3$, J. Phys. Conf. Ser. 200 (2010) 012014.
[14] B. Ramachandran, K.Z. Syu, Y.K. Kuo, A.A. Gippius, A.V. Shevelkov, V.Yu Verchenko, C.S. Lue, Thermoelectric performance of intermetallic $FeGa_3$ with Co doping, J. Alloy. Comp. 608 (2014) 229–234.
[15] M.S. Likhanov, V.Yu Verchenko, M.A. Bykov, A.A. Tsirlin, A.A. Gippius, D. Berthebaud, A. Maignan, A.V. Shevelkov, Crystalgrowth, electronic structure, and properties of Ni-substituted $FeGa_3$, J. Solid State Chem. 236 (2016) 166–172.
[16] K. Umeo, Y. Hadano, S. Narazu, T. Onimaru, M.A. Avila, T. Takabatake, Ferromagnetic instability in a doped band gap semiconductor $FeGa_3$, Phys. Rev. B 86 (2012) 144421.
[17] D.J. Singh, Itinerant origin of the ferromagnetic quantum critical point in $Fe(Ga,Ge)_3$, Phys. Rev. B 88 (2013) 064422.
[18] B. Koo, K. Bader, U. Burkhardt, M. Baenitz, P. Gille, J. Sichelschmidt, Spin dynamics of $FeGa_{3-x}Ge_x$ studied by electron spin resonance, J. Phys. Condens. Matter 30 (2018) 045601.
[19] Y. Zhang, J. Chen, J. Ma, J. Ni, M. Imai, C. Michioka, Y. Hadano, M.A. Avila, T. Takabatake, S. Li, K. Yoshimura, Transitions from a Kondo-like diamagnetic insulator into a modulated ferromagnetic metal in $FeGa_{3-y}Ge_y$, Proc. Natl. Acad. Sci. Unit. States Am. 115 (2018) 3273–3278.
[20] Y. Zhang, Y. Takahashi, M. Imai, G. Wang, M.A. Avila, T. Takabatake, C. Michioka, H. Ueda, K. Yoshimura, J. Ma, AIP Adv. 8 (2018) 101429.
[21] M.B. Gamża, J.M. Tomczak, C. Brown, A. Puri, G. Kotliar, M.C. Aronson, Electronic correlations in $FeGa_3$ and the effect of hole doping on its magnetic properties, Phys. Rev. B 89 (2014) 195102.
[22] A.A. Gippius, V.Yu Verchenko, A.V. Tkachev, N.E. Gervits, C.S. Lue, A.A. Tsirlin, N. Büttgen, W. Krätschmer, M. Baenitz, M. Shatruk, A.V. Shevelkov, Interplay between localized and itinerant magnetism in Co substituted $FeGa_3$, Phys. Rev. B 89 (2014) 104426.
[23] F.R. Wagner, R. Cardoso-Gil, B. Boucher, M. Wagner-Reetz, J. Sichelschmidt, P. Gille, M. Baenitz, Yu Grin, On Fe–Fe dumbbells in the ideal and real structures of $FeGa_3$, Inorg. Chem. 57 (2018) 12908–12919.
[24] Y. Takagiwa, Y. Matsuura, K. Kimura, Effect of carrier-doping on the thermoelectric properties of narrow-bandgap $(Fe,Ru)Ga_3$ intermetallic compounds, J. Electron. Mater. 43 (2016) 2206–2211.
[25] M. Wagner-Reetz, R. Cardoso-Gil, Yu Crin, Substitution solid solutions $FeGa_{3-x}E_x$ and their thermoelectric properties, J. Electron. Mater. 43 (2014) 1857–1864.
[26] V.Yu Verchenko, A.O. Zubtsovskii, A.A. Tsirlin, A.V. Shevelkov, Chemical pressure in the correlated narrow-gap semiconductor $FeGa_3$, J. Mater. Sci. 54 (2019) 2371–2378.
[27] G.R. Hearne, S. Bhattacharjee, B.P. Doyle, M.A.M. Ahmed, P. Musyimi, E. Carleschi, B. Joseph, Pressure-induced disruption of the local environment of Fe-Fe dimers in $FeGa_3$ accompanied by metallization, Phys. Rev. B 98 (2018), 020101(R).
[28] W. Xie, H. Luo, B.F. Phelan, T. Klimczuk, F.A. Cevallos, R.J. Cava, Endohedral gallide cluster superconductors and superconductivity in $ReGa_5$, Proc. Natl. Acad. Sci. Unit. States Am. 112 (2015) E7048–E7054.
[29] V. Petříček, M. Dusek, L. Palatinus, Crystallographic computing system JANA2006: general features, Z. Kristallogr. 229 (2014) 345–352.
[30] W.G. Clark, M.E. Hanson, F. Lefloch, P. Ségransan, Magnetic resonance spectral reconstruction using frequency-shifted and summed Fourier transform processing, Rev. Sci. Instrum. 66 (1995) 2453.
[31] M.S. Likhanov, V.Yu Verchenko, D.I. Nasonova, A.A. Gippius, S.V. Zhurenko, E.I. Demikhov, C.N. Kuo, C.S. Lue, B.L. Young, A.V. Shevelkov, Crystal structure and magnetic properties of intermetallic semiconductor $FeGa_3$ lightly doped by Co and Ni, J. Alloy. Comp. 745 (2018) 341–346.
[32] V.Yu Verchenko, M.S. Likhanov, M.A. Kirsanova, A.A. Gippius, A.V. Tkachev, N.E. Gervits, A.V. Galeeva, N. Büttgen, W. Krätschmer, C.S. Lue, K.S. Okhotnikov, A.V. Shevelkov, Intermetallic solid solution $Fe_{1-x}Co_xGa_3$: synthesis, structure, NQR study and electronic band structure calculations, J. Solid State Chem. 194 (2012) 361–368.
[33] S.V. Popova, L.N. Fomicheva, Inorg. Mater. 18 (1982) 205–208.
[34] I.V. Korolkov, A.I. Gubanov, S.A. Gromilov, Thermolysis of $[Pt(NH_3)_4][ReHlg_6]$ (Hlg= Cl, Br). Structure refinement for $[Pt(NH_3)_4][ReCl_6]$, J. Struct. Chem. 46 (2005) 479–487.
[35] B. Boucher, R. Al R. Al Orabi, B. Fontaine, Yu Grin, R. Gautier, J.-F. Halet, Enhancement of the thermoelectric properties of $FeGa_3$-type structures with group 6 transition metals: a computational exploration, Inorg. Chem. 56 (2017) 4229–4237.
[36] M. Wagner, R. Cardoso-Gil, N. Oeschler, H. Rosner, Yu Grin, $RuIn_{3-x}Sn_x$, $RuIn_{3-x}Zn_x$, and $Ru_{1-y}In_3$—new thermoelectrics based on the semiconductor $RuIn_3$, J. Mater. Res. 26 (2011) 1886–1893.
[37] M. Wagner-Reetz, R. Cardoso-Gil, Yu Prots, W. Schnelle, Yu Grin, Thermoelectric properties of single- and polycrystalline $RuGa_3$, Solid State Sci. 32 (2014) 56–60.
[38] D. Bogdanov, K. Winzer, I.A. Nekrasov, T. Pruschke, Electronic properties of the semiconductor $RuIn_3$, J. Phys. Condens. Matter 19 (2007) 232202.
[39] V. Ponnambalam, D.T. Morelli, Improved thermoelectric properties in heavily doped $FeGa_3$, J. Appl. Phys. 118 (2015) 245101.